Thermoelectric properties of Ru2TiGe Heusler phase

Sanchayita Mondal, Krishanu Ghosh, R. Ranganathan, Eric Alleno, Chandan Mazumdar

Thermoelectric properties of Ru_2TiGe Heusler phase

Sanchayita Mondal[a,b,*], Krishanu Ghosh[c], R. Ranganathan[b], Eric Alleno[d], Chandan Mazumdar[b,*]

[a] *Maharaja Manindra Chandra College, 20 Ramkanto Bose Street, Kolkata 700003, West Bengal, India*
[b] *Condensed Matter Physics Division, Saha Institute of Nuclear Physics, 1/AF, Bidhannagar, Kolkata 700064, India*
[c] *Department of Physics, P.C. Vigyan College, Kathari Bag Road, Chapra, 841301, Bihar, India*
[d] *Univ Paris Est Creteil, CNRS, ICMPE, UMR 7182, 2-8, rue H. Dunant, F-94320 THIAIS, France*

Abstract

We report a study of structural, magnetic, heat capacity and thermoelectric properties of a Ru-based Heusler alloy, Ru_2TiGe. The magnetic measurements reveal that at higher temperatures, diamagnetic and Pauli paramagnetic contributions dominate the magnetic behaviour whereas, at lower temperatures ($T \leq$ 20 K), superparamagnetic interaction among clusters is observed. The developement of such magnetism, however, does not exhibit any noticeable influence in thermoelectric properties. Though the temperature dependence of resistivity exhibits a metal-like nature, the large value of Seebeck coefficient leads to an appreciable power factor of the order of 0.54 mW/mK^2 at 300 K. Large power factor as well as low thermal conductivity results in a value of $zT = 0.025$ at 390 K for Ru_2TiGe that is orders of magnitude higher than that of the other pure Heusler alloys and point towards its high potential for practical thermoelectric applications.

1. Introduction

Power generation and refrigeration using thermoelectric devices are attracting more and more attention from researchers on a global scale due to their environment-friendly technology as well as long-term maintenance-free operation. The efficiency of a thermoelectric device in recovering waste heat depends on the figure of merit, zT ($zT = \frac{S^2T}{\rho\kappa}$, where S is the thermopower or Seebeck coefficient, ρ and κ are the electrical resistivity and thermal conductivity, respectively), of the thermoelectric material used in the device. However, most of the materials commercially available for use in thermoelectric devices, are known to be rather toxic and expensive as well as not efficient enough, which limit their practical applications [1, 2]. Therefore, to optimize the performance of a thermoelectric device, it is crucial to identify new thermoelectric materials with large zT. Recently, compounds like skutterudites [3], clathrates [4], and Heusler alloys families [5, 6, 7], *etc.* have been investigated for their potential as new thermoelectric materials. Among the different families of compounds, Heusler alloys have aroused great interest for the possibility of doping/substituting each of its constituting elements in order to optimize their physical properties [8].

Heusler alloys, X_2YZ (X/Y are primarily transition metals, rare earth metals or actinides, Z = a p-block element), crystallize in the cubic structure $L2_1$ having the space group: $Fm\bar{3}m$. The $L2_1$ structure consists of four interpenetrating face-centered cubic (*fcc*) sublattices where the X-atoms occupy the positions $(\frac{1}{4}\frac{1}{4}\frac{1}{4})$ and $(\frac{3}{4}\frac{3}{4}\frac{3}{4})$, while Y and Z atoms are located at the positions $(\frac{1}{2}\frac{1}{2}\frac{1}{2})$ and (0 0 0), respectively [8, 9]. Interestingly, many different properties of Heusler alloys can be uniquely controlled by their valence electron counts (VEC). Heusler compounds having VEC 24 have shown promise for thermoelectric applications due to their semiconducting or semi-metallic ground state. Starting with Fe_2VAl [10], many new Heusler

*Corresponding authors
Email addresses: sanchayita.mondal87@gmail.com (Sanchayita Mondal), chandan.mazumdar@saha.ac.in (Chandan Mazumdar)

alloys (Fe_2VGa, Fe_2TiSn *etc.* [11, 12]) having VEC 24 have been discovered and studied so far in search of large zT. The main challenge one usually faces while identifying a good thermoelectric material is to decrease the thermal conductivity and improve the power factor (PF = S^2/ρ) at the same time. It was found that in case of Fe_2VAl, the lattice thermal conductivity could be significantly reduced by doping/substitution with a heavier element [13]. By extending this idea, one would therefore be tempted to use heavier elements to identify and synthesize new Heusler materials, maintaining the number of valence electrons at 24. As Ru is isoelectronic to Fe and has a larger atomic mass, the existence of some Ru-based Heusler alloys having a VEC 24 have been reported recently. Among those alloys, a semi-metallic ground state has been observed in Ru_2NbAl [14], Ru_2NbGa [15] and Ru_2TaAl [16] while Ru_2VZ (Z = Al, Ga) [17, 18, 19] shows metallic behaviour. Although having semi-metallic ground state, only Ru_2NbAl among the pristine compounds showed an appreciable value of zT at 300 K (zT_{300K} = 0.0052) [14]. Even though most Ru-based compounds exhibit relatively low thermal conductivity compared to that of Fe-based Heusler alloys, the difficulties in achieving high zT lie in their low values of thermopower. Among these Ru-based alloys, a recent theoretical study predicted that Ru_2TiGe would be a potentially good thermoelectric material [20] because it presents the possibility of having a high thermopower as well as a semi-metallic ground state, which are necessary for practical use. In comparison to Fe_2VAl, Ru_2TiGe contains two heavier elements, *viz.*, Ru and Ge, while the atomic weights of V and Ti are almost comparable.

In addition to their potential as good thermoelectric material, Heusler alloys are also known to exhibit many intriguing magnetic properties. Interestingly, the total magnetic moment (M) per unit cell of a Heusler material can be estimated using the Slater-Pauling rule: $M(\mu_B)$ = |VEC−24| [21]. Thus, Heusler alloys with VEC 24 should be non-magnetic with zero total magnetic moment per unit cell. Several materials with VEC 24 are indeed found to be non-magnetic [10, 22, 23]. Nevertheless, close inspections of experimental measurements of the magnetic properties of these alloys reveal that many of the reported compounds could even be classified as marginally magnetic instead, and in some cases the reported deviation in magnetic behavior have also been explained differently by different investigators. For example, while one study reported cluster glass behavior for Fe_2VAl [24], other studies revealed the presence of superparamagnetism (SPM) or even ferromagnetism [25, 26]. SPM is also observed in other Heusler alloys based on Fe and Ru having VEC 24, namely Fe_2VGa, Ru_2NbAl, *etc.* [11, 14]. Some other compounds of this class, *e.g.*, Fe_2TiSn, Ru_2NbAl *etc.* [14, 27] also exhibit ferromagnetic interactions. It is generally accepted that most of these various magnetic behaviors are due to the antisite type structural defects that usually develop during the synthesis and annealing process. Thus, a thorough study of the magnetic properties of Ru_2TiGe could also help us to understand the microstructural aspects which in turn can influence the thermoelectric properties.

In the present work, we therefore report a detailed study on Ru_2TiGe through structural, magnetic, heat capacity as well as thermoelectric measurements. It should be noted here that although none of the constituting elements usually considered to be magnetic, our study reveals the presence of superparamagnetically interacting aggregates in Ru_2TiGe, most likely originating from antiste defects detected in the material. Thermoelectric measurements suggest that despite a metal-like ground state, a relatively large thermopower can be observed in this compound, leading to a zT value of about 0.025 at 390 K, the highest among undoped Heusler alloys yet reported.

2. Experimental methods

A polycrystalline Ru_2TiGe ingot was synthesized by arc melting technique under flowing Ar atmosphere. Stoichiometric amounts of the constituent elements Ru (>99.9%), Ti (>99.99%) and Ge (>99.9999%) were melted several times to achieve homogeneity. The weight loss in this process was observed to be less than 0.5%. The as-cast ingot was then wrapped in Ta-foil and annealed at 1273 K for 48 hours in a vacuum-sealed quartz tube followed by quenching in ice-water. The sample was annealed again at 1223 K for 12 hours after cleaning its surface and following the same quenching procedure. The ingot was then cut in appropriate shapes and polished and again annealed for 2 hours at 1173 K following the similar procedure to eliminate the surface strain that might have been generated due to the mechanical stress in the process of

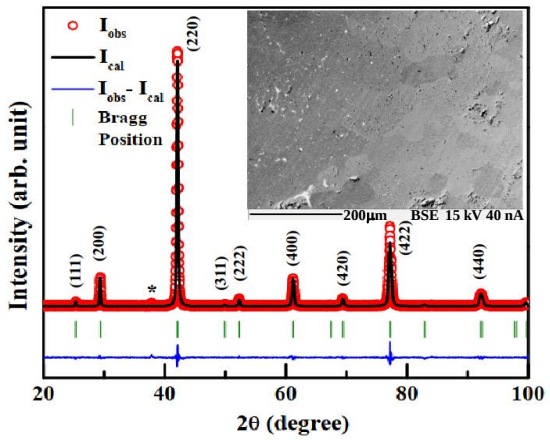

Figure 1: Powdered X-ray diffraction pattern of Ru_2TiGe, measured at room temperature & indexed considering the $L2_1$ crystal structure. Presence of minor amount of unreacted Ru is marked by * symbol. Inset: Back scattered image of Ru_2TiGe.

scraping, cutting and polishing, as some Heusler alloys are observed to be highly sensible to such coldwork [28, 29]. The sample homogeneity and chemical composition of the annealed sample were evaluated by using the Wavelength Dispersive Spectroscopy based Electron Probe Micro-Analysis (WDS-EPMA) technique [Model: SX 100, M/s Cameca, France]. The powdered X-ray diffraction (XRD) technique was adapted to check the single phase nature of Ru_2TiGe at 300 K using Cu K_α radiation in a powder diffractometer equipped with a rotating anode X-ray source at 9 kW [Model: TTREX III, M/s Rigaku Corp., Japan]. The XRD measurements were further carried out down to 12 K in order to look for any probable structural distortion. The Rietveld refinement technique by using FULLPROF software [30] is used to analyze the XRD patterns. Thermal transport [$\rho(T)$, $S(T)$, $\kappa(T)$], heat capacity [C], Hall coefficient [R_H] and magnetic [$M(T, H)$] properties were measured using commercial set ups [Models: PPMS Evercool-II and SQUID-VSM, M/s Quantum Design Inc., USA]. For transport measurement we have used a long rectangular shaped sample piece.

3. Results and Discussion

3.1. Structural details

The XRD pattern of Ru_2TiGe taken at 300 K is shown in Fig. 1. All the diffraction lines except a peak with negligible intensity ($\sim 1\%$ of most intense peak) at $2\theta \sim 37°$, can be indexed considering the $L2_1$ crystal structure (Fig. 1). The lattice parameter estimated to be 6.034(1) Å, matches well with the earlier reported value of 6.035 Å [31]. The extra peak at $2\theta \sim 37°$, appeared due to the presence of a negligible amount of unreacted Ru, and have earlier been reported in many other Ru-based Heusler compounds [15, 31]. Another secondary phase was detected by EPMA (white areas in the inset of Fig. 1), where localized analysis found $Ru_{1.06}Ge_{0.94}$ as an apparent composition, most likely corresponding to the RuGe-Ru eutectic reported in the binary Ru-Ge phase diagram [32]. However, the Bragg peaks associated with the RuGe phase can not be seen in the XRD pattern of Ru_2TiGe. One of the possible reason for the visual absence of the Bragg peaks of RuGe is that the compound forms in cubic B2-type crystal structure, whose lattice parameter (a = 3.011 Å) is nearly half of that of Ru_2TiGe (a = 6.034 Å that can be expressed as 2×3.017 Å). As a result, the Bragg peaks from both the compound could overlap with each other, and can not be resolved separately. The presence of such small fraction of Ru as a secondary phase in these materials has been argued to have no influence in their transport and magnetic properties at all [15, 31]. Similarly, we argue here that a minute fraction of non-magnetic and metallic RuGe [33] does not affect the physical properties of Ru_2TiGe either. It may also be noted here that the signature of structural antisite disorder is frequently observed

Table 1: Crystallographic parameters of Ru_2TiGe obtained from the Rietveld refinement.

Ru_2TiGe	
Structure	Cubic $L2_1$
Space group	$Fm\bar{3}m$, No. 225
Lattice parameter	6.034(1) Å
Element	Occupancy
Ge ($4a$: 0,0,0)	0.986
Ti ($4b$: $\frac{1}{2}, \frac{1}{2}, \frac{1}{2}$)	1.000
Ru ($8c$: $\frac{1}{4}, \frac{1}{4}, \frac{1}{4}$)	1.944
R_p	3.61 %
R_{wp}	5.15 %
Volume	219.69(2)
Density	9.79 g/cm^3

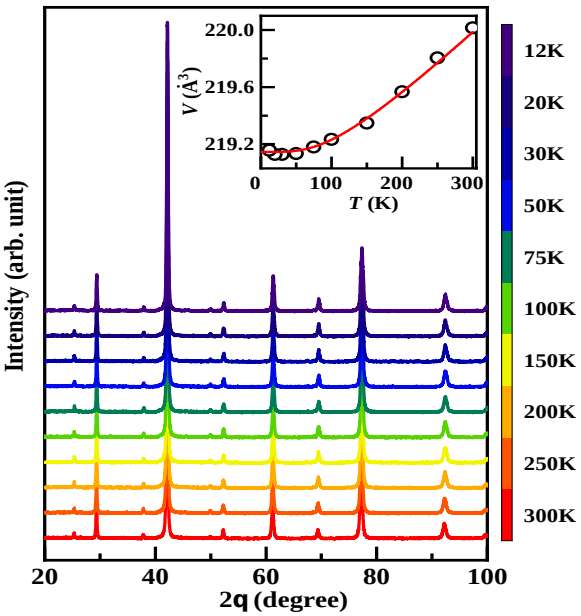

Figure 2: Low temperature XRD pattern of Ru_2TiGe down to 12 K; Inset: Temperature dependence of unit-cell volume of Ru_2TiGe. Solid line represents a fit to Eq. 1.

in the Heusler compounds in perturbation to the ordered $L2_1$ phase. When Y and Z atoms exchange their respective positions and distribute evenly, the B2 type disordered state is resulted. The occurrence of B2 phase is generally reflected in the XRD pattern by diminished intensity of (111) diffraction line. In case of Ru_2TiGe forming in the ordered $L2_1$ crystal structure, the intensity of (111) peak is calculated to be 2 % of the most intense line. In the present diffraction pattern, the measured intensity of the said diffraction line is ∼1.9 % suggesting the sample is primarily forming in the ordered $L2_1$ phase. The elemental composition of the matrix, derived from the EPMA measurements is $Ru_{1.91(1)}Ti_{1.05(3)}Ge_{1.03(3)}$. This deviation from the stoichiometry is in agreement with the occurrence of Ru and RuGe secondary phases and also indicates the presence of Ti_{Ru} and Ge_{Ru} antisite defects where some of the Ti (Y) and Ge (Z) atoms occupies Ru (X) sites.

The XRD patterns collected at different temperatures between 300 K to 12 K do not show any detectable change in primary diffraction pattern-type indicating that the crystal structure remains unaltered down to 12 K, the lowest temperature achievable in our diffractometer (Fig. 2). The lattice parameter gradually decreases with decreasing temperature similar to that observed in most of the materials. The unit-cell volume of Ru_2TiGe is plotted as a function of temperature and fitted (Fig. 2, inset) using the following equation [34]

$$V(T) = \gamma_G U(T)/K_0 + V_0, \qquad (1)$$

where V_0 represents the unit-cell volume at $T = 0$ K, K_0 is the bulk modulus, and γ_G is the Grüneisen parameter. *U(T)*, the internal elastic energy can be described by considering the Debye approximation as

$$U(T) = 9NK_BT\left(\frac{T}{\Theta_D}\right)^3 \int_0^{\frac{\Theta_D}{T}} \frac{x^3}{e^x - 1}dx \qquad (2)$$

where N is the number of atoms per unit cell and $x = \hbar\omega/k_B T$. From the fit of *V(T)* curve of Ru_2TiGe, the Debye temperature Θ_D and the Grüneisen parameter γ_G are estimated to be 400 K and 1.6, respectively. The theoretically calculated value of K_0 =228 GPa [35] is used for the estimation of γ_G.

3.2. Magnetic properties

3.2.1. Magnetic susceptibility

The temperature dependence of magnetic susceptibility [$\chi(T)$] behaviour of Ru_2TiGe has been investigated applying external magnetic field (H) of strengths 10 kOe and 70 kOe. The susceptibility values measured under zero field cooled (ZFC) and field cooled (FC) protocols at 10 kOe do not show any thermoremanence behaviour. The values of $\chi(T)$ at 10 kOe found to be very small though remain positive throughout the whole temperature region (Fig. 3, top). In contrast, the susceptibility values measured at 70 kOe become negative (Fig. 3, bottom) in the intermediate temperature range (100–200 K) suggesting the presence of diamagnetism in Ru_2TiGe. However, a minor upturn could be seen in the $\chi(T)$ curves for both the fields at higher temperatures, indicating Pauli paramagnetic (PPM) behaviour.

Experimentally observed $\chi(T)$ curves can be well explained considering a modified Curie-Weiss equation [36], expressed as

$$\chi(T) = \frac{C}{T - \theta_p} + \chi_0 + \alpha T^2, \qquad (3)$$

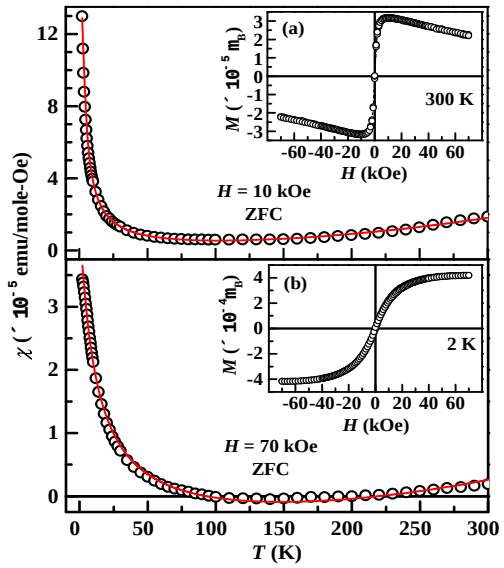

Figure 3: Temperature dependence of magnetic susceptibility of Ru_2TiGe measured at (top) H = 10 kOe and (bottom) 70 kOe under ZFC configuration along with a fit to Eq. 3; Insets: Isothermal magnetization at (a) 300 K and (b) 2 K of the same sample.

where the first term is the well known Curie-Weiss expression, χ_0 is temperature independent diamagnetic (χ_{dia}) and/or Pauli paramagnetic (χ_{PPM}) contributions and αT^2 is the higher order term in the expanded Pauli paramagnetic equation which is generally neglected in the zeroth order approximation [36]. Using Eq. 3, the ZFC susceptibilities for both 10 kOe and 70 kOe applied field have been fitted and the fit parameters are shown in Table 2. The values of χ_0 for both the fields are found to be negative suggesting the predominant magnetic contribution is diamagnetic in Ru_2TiGe. It may be noted that the temperature independent contribution, χ_0, was reported to be positive in the earlier preliminary magnetic susceptibility analysis for the same compound measured under 10 kOe field [37]. However, it may be pointed out that the analysis method appears to be quite different, as the earlier report might not have considered the higher order αT^2 term. As the earlier report did not present any detailed analysis, except mentioning it to be paramagnetic, it is not possible to compare the magnetic properties presented in this work with that reported earlier [37]. The finer details could be different due to their synthesis condition and resulting differences in inherent

Table 2: Parameters extracted from the fit of ZFC $\chi(T)$ curves for H = 10 kOe and 70 kOe to Eq. 3 for Ru_2TiGe.

H (kOe)	χ_0 (emu/mol-Oe)	μ_{eff} (μ_B)	θ_p (K)	α (emu/mol-Oe-T^2)
10	-0.75×10^{-6}	0.058	−1.32	1.93×10^{-10}
70	-6.32×10^{-6}	0.069	−11.85	0.78×10^{-10}

microstructures. In the present study, the magnetic susceptibility measured at 70 kOe, however resulted in a higher absolute value of χ_0, revealing that effect of Pauli paramagnetic contribution has been suppressed on applying higher field. Our estimated values of χ_0 are the resultant of these two components, *viz.*, positive Pauli paramagnetic and negative diamagnetic ($\chi_0 = \chi_{PPM} - \chi_{dia}$). Apart from these two contributions, very small values of effective paramagnetic moment (μ_{eff}) and paramagnetic Curie temperature (θ_p) point towards the presence of another additional short range magnetic component, effect of which is evident in the relatively sharp upturn in χ-T curves at low temperatures below $\sim$ 25 K (Fig. 3). Such additional magnetic contribution may have been originated from the discernible deviation of stoichiometry that leads to small percentage of Ti_{Ru} and Ge_{Ru} antisite defects in this compound. It should be pointed out here that appearance of magnetic contribution from these defects is although rare, yet similar short range magnetization have earlier been reported in quite a few compounds *e.g.*, Ru_2NbAl [14], $SrRuO_3$ [38] *etc.*, where none of the constituent elements are generally considered to be magnetic in nature. Effect of those defects and disorders in Ru_2TiGe are further explored through isothermal magnetization measurements described below.

3.2.2. Isothermal magnetization

In order to further understand the magnetic behaviour of Ru_2TiGe, the isothermal magnetisation data have been collected at different temperatures as a function of externally applied magnetic field. The magnetic isothermal [*M(H)*] curve, taken at 300 K [Fig 3, inset(a)], increases initially upon increasing magnetic field up to 10 kOe after which the slope of the curve changes and becomes negative throughout the remaining magnetic field range scanned (10 < H

$\leq$ 70 kOe). Such magnetic behaviour could be a result of simultaneous presence of two different type of magnetic contributions; one having positive magnetization and other with a negative component. Generally, negative magnetization has its origin in the diamagnetic contribution which varies linearly with increasing applied magnetic field, yielding a negative slope. To explain the non-linear variation of the isothermal magnetization, the positive component of magnetisation must be non-linear. If different magnetic interactions contribute towards this positive magnetisation, at least one such contribution should be non-linear, in order to maintain the non-linearity of overall magnetisation. The positive contribution in this case increases rapidly with increasing applied field up to 10 kOe and then must have approached a saturating tendency suggesting that the positive contribution either could be of ferromagnetic type or a combination of paramagnetic and ferromagnetic interactions. In contrast, the isothermal magnetization at 2 K increases slowly with applied field and shows a approach-to-saturation-like behaviour [Fig 3, inset(b)]. In both the isotherms, taken at 300 K and 2 K, no hysteresis behaviour were observed. Since, signature of any ferromagnetic long range order could not be detected in the susceptibility behaviour of Ru_2TiGe, the presence of a subtle ferromagnetic contribution in the magnetic isotherm taken only at 300 K could possibly be generated from an impurity phase, present beyond the detection limit of both the XRD as well as EPMA analysis performed on this material. Elemental Fe could be a possible candidate for the impurity phase as it also saturates near 10 kOe though its saturation magnetisation, 2.2 μ_B, is much higher than the observed value ($\sim 3\times10^{-5}$ μ_B at 10 kOe) at 300 K in Ru_2TiGe. Considering the whole positive contribution to the *M(H)* curve at 300 K is the manifestation of Fe impurity in Ru_2TiGe, the amount of Fe present in the system is estimated to be 0.0015 % or 15 ppm (parts per million). To avoid such percentage of impurity, one need to prepare sample with all the starting elements having purity >99.9985%. Although for the synthesis of Ru_2TiGe, we have used Ti and Ge having purity >99.9985%, the purity of Ru was limited to 99.9%. Thus, 99.9% pure Ru available to us might easily be the source of the minuscule Fe impurity discussed above. Such a small impurity would also remain beyond the detection limit of measurements like XRD, EPMA, *etc.* employed in this study. However, it may be noted here that aforesaid impurity has a visible influence mostly at higher temperatures, where the positive paramagnetic contribution of Ru_2TiGe is quite low and the diamagnetic contribution dominates. In addition, this diamagnetic contribution also has a very weak dependence (negative *dM/dH*) of magnetic field. On the other hand, the magnetization of the FM impurity has a rather large positive *dM/dH* in the low field region, but the magnetization saturates as the magnetic field increases. As a result, the effect of FM impurity, though of very tiny fraction, has an overwhelming influence in the low field region. Once the FM contribution to isothermal magnetization saturates at higher field, the negative *dM/dH* of the diamagnetic contribution starts to manifest its domination. In contrast, at 2 K, the inherent magnetization value is quite large, increases as the magnetic field is raised and reaches toward a magnetization value $\sim 4\times10^{-4}$ μ_B at 70 kOe, which is one order of magnitude higher than that of the FM impurity. Such larger magnetization values suppress the manifestation of magnetic impurity effect at the low temperature isothermal magnetization result. Similar presence of elemental magnetic impurity is also reported earlier in literature [39]. Such type of impurity, however, have very little effects in their transport properties. It may be pointed out here that the effect of such FM impurity does not have any significant influence on the $\chi(T)$ data taken at 10 kOe and 70 kOe in the temperature range 2–300 K, presented in the previous section. The measured temperature range is well below the FM ordering temperature of Fe (1043 K) and both the applied magnetic fields (10 kOe and 70 kOe) falls within the magnetic saturation region of the isothermal magnetization characteristics of the Fe impurity. Thus the minute presence of the said Fe impurity can only contribute a very small positive temperature independent term ($\sim10^{-}6$ emu/mol-Oe) to the $\chi(T)$ curves. The effect of removal of such constant term from each $\chi(T)$ curves only results in a bit higher χ_0 values than that given in Table 2.

To check the slope of the *M(H)* curve at intermediate temperatures, the data have also been taken at 20 K, 15 K, 10 K, and 5 K (Fig 4). It is observed that for all the temperatures the magnetic isotherms are nonlinear and show positive slopes.

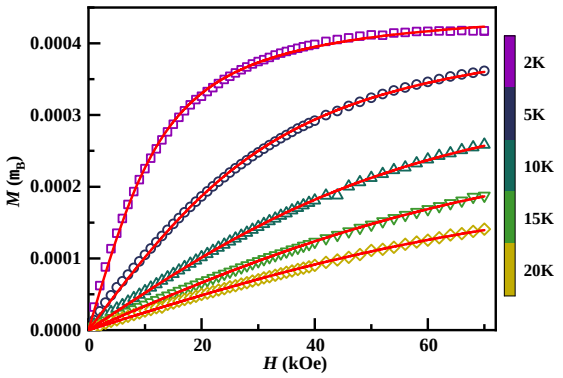

Figure 4: Isothermal magnetization data at various temperature for Ru_2TiGe. The solid lines represent the fit of the data using Eq. 4.

The nonlinearity increases as the temperature decreases. Since the susceptibility behaviour negate the possibility of the presence of any long range ordering in this compound, the deviation from the linear nature of the magnetic isotherms (expected in purely paramagnetic system) indicate towards the presence of a short range interaction. Generally, such S-shaped anhysteretic behaviour is observed in the materials having short range ferromagnetic interactions or a superparamagnetic (SPM) state.

To find the origin of the approach to such saturation-like behaviour, we have analyzed all the *M(H)* curves below 20 K considering the presence of SPM state in this material. To properly assign SPM to any system, two different conditions need to be simultaneously satisfied. Firstly, S-shaped anhysteretic curves should be described by a Langevin function and secondly, all the magnetic isotherms in the temperature range where the superparamagnetism is manifested, should overlap in a universal curve when plotted as a function of H/T [40]. We found that all the *M(H)* curves below 20 K can be well-explained using the Langevin function [24, 25], given by

$$M(H) = M_S L(x) \tag{4}$$

where $x = \frac{\mu H}{k_B T}$, M_S is the saturation magnetization, μ represents the average magnetic moment per cluster and $L(x) = coth(x) - 1/x$, is the Langevin function. The parameters extracted from the fits are listed in Table 3. It can be observed that for all the temperature in the region 20 K to 2 K, the magnetic moment per SPM cluster shows a little variation around ∼6 μ_B. The saturation magnetization and the number of SPM cluster per mole are estimated to be ∼ 4×10^{-4} μ_B/f.u. and ∼ 10^{20}/mole and are found to be close enough in the temperature range from 2–20 K. In order to check the other condition, all the magnetic isotherms below 20 K are plotted as a function of H/T (Fig. 5). Interestingly, it can be seen that they all indeed follow a single universal curve, confirming the presence of SPM in Ru_2TiGe below 20 K. It can be concluded from the analysis of the isothermal magnetization of Ru_2TiGe that the superparamagnetically interacting clusters develop below 20 K, whereas a competition between diamagnetic and ferromagnetic contributions is apparent at the higher temperatures.

A similar or comparable magnetic feature is not restricted to Ru_2TiGe, but also found in quite a few other Heusler alloys including Ru_2NbAl [14], Fe_2VAl [25], *etc.* having VEC 24. In case of Fe_2VAl, it was shown that the local perturbation caused by the Fe_V and Fe_{Al}-type antisite disorders result in the development of unpaired *d*-electron and the observed magnetism in that material is the direct outcome of those unpaired electrons belonging to the region containing antisite defects [8, 41]. As the theoretical calculation was carried out considering the atomic disorders within the basic $L2_1$-cubic structure, this particular crystal structure certainly play a major role in such magnetism [8, 41]. However, the development of such unpaired electron need not be restricted to any particular chemical composition, as long as the compound is forming with transition metal elements. For Ru_2NbAl too, the magnetism was also argued to have originated from Ru_{Nb} and Al_{Nb}-type local disorders [14]. In the present case of

Table 3: The parameters, μ and M_s, obtained from fitting of isothermal magnetisation at different temperatures, T, using Eq. 4 are presented here. Number of SPM cluster per f.u. (M_s/μ) and per mole ($N = \frac{M_s}{\mu} \times 6.023\times10^{23}$) are also given.

T (K)	μ (μ_B)	M_s ($\times10^{-4}\mu_B$/f.u.)	M_s/μ ($\times10^{-5}$/f.u.)	N ($\times10^{20}$/mole)
2	5.29	4.61	8.71	0.52
5	5.16	4.54	8.80	0.52
10	5.94	3.96	6.67	0.40
15	6.80	3.33	4.90	0.29
20	2.14	2.58	2.14	0.12

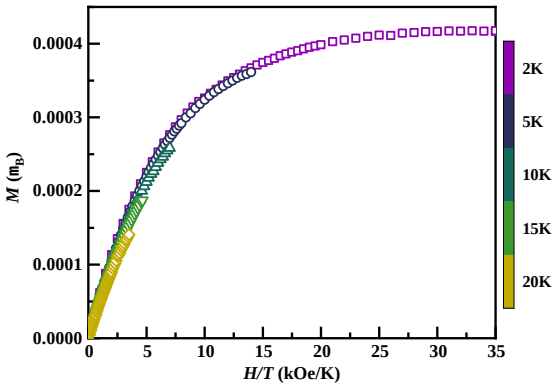

Figure 5: The SPM state follows universal curve at low temperature isotherm for Ru_2TiGe.

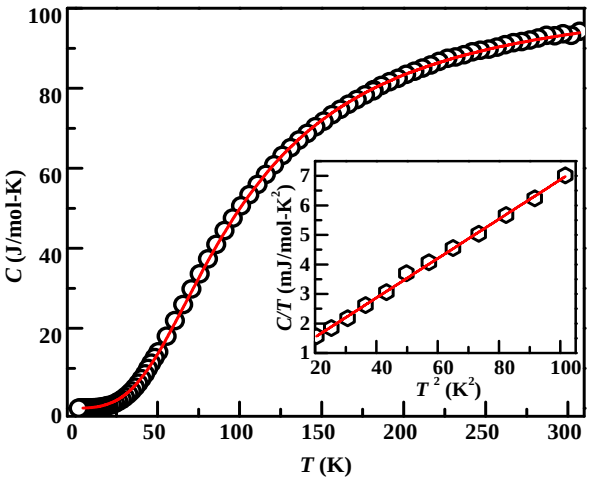

Figure 6: Specific heat as a function of temperature of Ru_2TiGe. Solid line represents the fit to Eq. 5; Inset: C/T vs T^2 plot at low temperatures along with the fit to Eq. 6.

Ru_2TiGe, development of Ti_{Ru} and Ge_{Ru}-types of antisite disorders have also been inferred from the XRD as well as EPMA measurements. The superparamagnetic behaviour in this material thus also likely to have originated due to the formation of small magnetic clusters around those defects.

3.3. Heat capacity

To ensure the veracity of the magnetization measurements, another independent experimental technique, the heat capacity [*C(T)*] has been carried out in the temperature range 2–300 K for Ru_2TiGe in absence of any external magnetic field (Fig. 6). The *C(T)* curve starts to increase as the temperature raises and does not show any signature of long range magnetic order supporting the results inferred from the magnetic measurements.

Generally, the observed heat capacity behaviour can be explained considering the Debye-Sommerfeld equation [42], given by,

$$C(T) = \gamma_S T + 9nR\left(\frac{T}{\Theta_D}\right)^3 \int_0^{\frac{\Theta_D}{T}} \frac{x^4 e^x}{(e^x-1)^2} dx \quad (5)$$

where $\gamma_S T$ is the electronic specific heat and the second term represents the lattice/phonon contribution to the heat capacity. The Sommerfeld coefficient $\gamma_S = \frac{1}{3}\pi^2 D(E_F) {k_B}^2$, where $D(E_F)$ is the density of states at the Fermi level, E_F and n represents the number of atoms per formula unit (for Ru_2TiGe: $n = 4$), Θ_D is the Debye temperature and $x = \hbar\omega/k_B T$. This above discussed Debye-Sommerfeld model could reproduce well the heat capacity data in the temperature range 35–300 K. The value of Θ_D and γ_S estimated from the fit are 407 K and 7.6 mJ/mol-K^2 respectively. The value of Θ_D is found similar to that obtained from the fit of lattice volume as a function of temperature (Sec. 3.1). A close inspection at the lower temperatures however reveals that the fit is not as good as it is in the higher temperatures and this is also reflected in the relatively high estimated value of γ_S comparing standard metallic system [42]. This value of γ_S, obtained from the fitting of heat capacity data to Eq. 5, is not proper as γ_S is generally a low temperature phenomenon [42] and thus a proper analysis of heat capacity data at lower temperature is crucial.

In the low temperature region Eq. 5 can be simplified as

$$C(T) = \gamma_S T + \beta T^3 + \delta T^5 + \cdots\cdots \quad (6)$$

where β, δ are the coefficients. Below $\sim \Theta_D/50$, δT^5 and other higher order terms could be neglected and the heat capacity behavior in the representation of C/T vs. T^2 is expected to show a linear dependance. The Debye temperature can be estimated from the slope (β) of such straight line: $\beta = (12\pi^4/5)Nk_B/{\Theta_D}^3$. It may be mentioned here that in some related off-stoichometric Heusler alloys [43, 44], the C/T vs. T^2 representation are known to deviate from linearity, although it remain lienar in Ru_2TiGe as expected in standard materials (Fig. 6, inset). The value of γ_S and β are found to be 0.2 mJ/mol-K^2 and 0.067 mJ/mol-

K^4 respectively. The value of Θ_D, calculated using obtained β is 487 K, found to be higher than that estimated from the whole temperature range fit. It is primarily because Θ_Ds, extracted using Debye-Sommerfeld equation, are known to have a small temperature dependence [45, 46]. In the Debye model, it was assumed that only low-frequency modes of lattice vibrations *i.e.*, acoustic modes contributes to the lattice specific heat for the large temperature region although this assumption is actually valid only at low temperatures. Therefore, at very low temperature, Θ_D should be temperature independent. As the temperature increases, not only the acoustic modes, but optical modes of lattice vibrations also found to contribute to the lattice specific heat that in turn decreases the value of Θ_D at higher temperature. Generally, the variations of Θ_D remain within 10% around their mean value for most of the elements, though some exceptions, for instance, 20% variations have also been observed in case of zinc, cadmium *etc.* [45, 46]. For general use, the value of Θ_D (Θ_D = 407 K for Ru_2TiGe), estimated from fit of the *C(T)* data in the temperature range 2–300 K should have better acceptability as it is averaged over the entire temperature region. The low but non-zero value of γ_S in Ru_2TiGe reveals that only a small number of free carriers are available for the electric conduction for this material, yielding a bad metal-like/semi-metallic ground state.

3.4. Transport properties

3.4.1. Electrical resistivity

The electrical resistivity behaviour as a function of temperature [$\rho(T)$] of Ru_2TiGe has been studied in the temperature range 2–390 K, shown in Fig. 7. The $\rho(T)$ curve exhibits a positive temperature coefficient of resistivity (TCR) over a large range of temperatures from 40 K to 390 K, suggesting metallic nature, similar to that found earlier on another experimental observation [37]. However, the experimental result found to be in contravention to the theoretical investigation of band structure calculations of Ru_2TiGe [20, 47] that had predicted the possibility of having a pseudo-gap ∼200 meV, which would have manifested in a semiconductor-like temperature dependence of resistivity. This deviation of $\rho(T)$ could be attributed to the structural antisite defects and disorders, noticed in this compound. The excess Ti-*d* and Ge-*p* bands originated from the Ti_{Ru} and Ge_{Ru} types of antisite

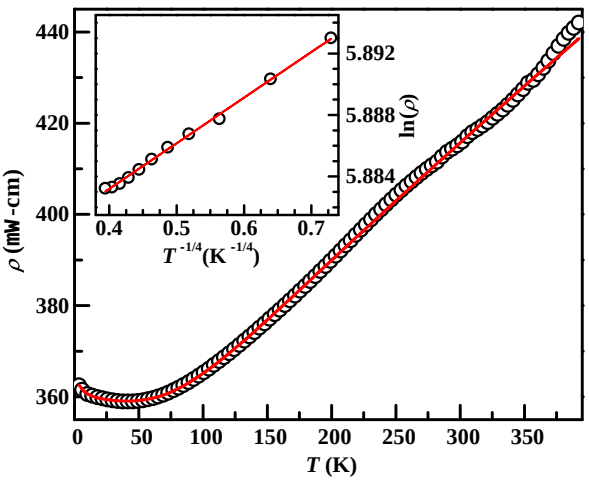

Figure 7: Resistivity as a function of temperature for Ru_2TiGe with a fit to Eq. 9; Inset: Plot of ln(ρ) vs. $T^{-1/4}$ below 40 K.

defects are likely to introduce additional states in pseudo-gap region leading to a metal-like $\rho(T)$ behaviour, as experimentally observed in Ru_2TiGe. The magnitude of ρ at 390 K is 443 $\mu\Omega$-cm whereas at 2 K it is found to be 362 $\mu\Omega$-cm giving a residual resistivity ratio (RRR = ρ_{390K}/ρ_{2K}) value of ∼ 1.22. Despite having a metal-like resistivity, where resistance decreases with decreasing temperature, low value of RRR suggests Ru_2TiGe to be a bad metal. A close inspection at the lower temperatures reveals that the TCR changes its sign from positive to negative at around 40 K and remain negative down to lowest measured temperature. It may be noted here that in systems having high resistances, sharp upturn at low temperature may arise from different quantum interference effects such as weak-localization, electron-electron interactions *etc.* [48, 49, 50]. Though $\rho(T)$ curve of Ru_2TiGe exhibits negative TCR below 40 K, the value of ρ changes at a very slow rate. Thus, the above mentioned processes may not be the primary basis of the negative TCR in Ru_2TiGe. We have discussed earlier that the structural analysis of Ru_2TiGe suggests small presence of Ti_{Ru} and Ge_{Ru} antisite defects. Such structural defects are often argued to be responsible for the localization of charge carriers [51]. Mott's variable range hopping (VRH) [52] of electrons between exponentially localized states is a mechanism that could explain both the negative TCR and high value of ρ in such systems at low temperature. In this mechanism, the conduction is expected to propagate via electrons, hopping

between localized sites that are energetically closed but not necessarily close in space. The conduction behaviour of VRH in three dimensional systems can be expressed as

$$\rho(T) = \rho_0 exp\left[\left(\frac{T_0}{T}\right)^{1/4}\right] \quad (7)$$

where ρ_0 represents the residual resistivity and T_0, the activation temperature, depends on the localization length (ξ) as ξ^{-3} [52]. The resistivity data of Ru_2TiGe has been plotted as $\ln(\rho)$ *vs.* $T^{-1/4}$ below 40 K (Fig. 7, Inset) and fitted using Eq. 7. In spite of having an excellent fit, the value of T_0 is found to be extremely low $\sim 7\times10^{-7}$ K than that of the values reported in the literature [14, 53] thus also ruling out the possibility of any significant role of VRH mechanism in this material.

On the other hand, it may be noted here that the magnetic measurements discussed earlier suggest the development of superparamagnetically interacting clusters in the low temperature region in this material. In many non-magnetic systems containing a minute magnetic impurity, such resistivity minimum at low temperatures is found to be originated from the Kondo effect [44, 54, 55]. Recently, in some strongly correlated manganites as well as ferromagnetic metals, the Kondo effect is observed [56, 57, 58]. According to Kondo's theory, the resistivity below the minimum increases following the relation: $\rho_{\rm Kondo} = \rho_0 - \rho_s \ln T$, where ρ_0 is the residual resistivity, the second term is the contribution from the interaction between the conduction electrons and the magnetic spins and ρ_s represents the strength of the Kondo spin scattering [54]. Therefore, it appears that the negative TCR in Ru_2TiGe could be attributed to the formation of those magnetic clusters, pointing towards the Kondo-scattering mechanism. The $\rho(T)$ behaviour above 40 K is almost linear and can be described using the Bloch-Grüneisen model [59] that considers the scattering of conduction electrons by the acoustic lattice vibrations. The temperature-dependent electrical resistivity of a metal according to the Bloch-Grüneisen model is given by

$$\rho_{\rm BG}(T) = \rho_{\Theta_{\rm D}}\left(\frac{T}{\Theta_{\rm D}}\right)^5 \int_0^{\frac{\Theta_{\rm D}}{T}} \frac{x^5}{(e^x-1)(1-e^{-x})}dx \quad (8)$$

where, $\rho_{\Theta_{\rm D}}$ is the value of resistivity at Debye temperature. In order to fit the $\rho(T)$ curve for the entire temperature region, the following equation has been used combining both Kondo effect and the Bloch-Grüneisen formula

$$\rho(T) = \rho_0 - \rho_s \ln T + \rho_{\rm BG}(T) \quad (9)$$

The $\rho(T)$ curve for Ru_2TiGe fitted very well using the above equation (Fig. 7). The parameters extracted from the fit are $\Theta_{\rm D}$ = 508 K, $\rho_{\Theta_{\rm D}}$ = 110 $\mu\Omega$-cm, ρ_0 = 361 $\mu\Omega$-cm and ρ_s = 1.1 $\mu\Omega$-cm. It may be noted here that the value of ρ_s, estimated above is relatively smaller in comparison to that reported in many magnetically ordered or glassy systems [57, 60], although even smaller values of ρ_s are also reported in some other Heusler compounds, *e.g.*, $Fe_2VAl_{1-x}B_x$ [56]. It may nevertheless be pointed out that although the magnitude of ρ_s, estimated for Ru_2TiGe, appears to be quite reasonable, the absence of any signature of Kondo scattering in the heat capacity data at low temperature cast a serious doubt on the possibility of Kondo scattering in this compound. Thus, the negative TCR, observed at the lower temperatures could also be a manifestation of the semiconductor nature of conductivity, as expected in VEC 24 Heusler alloys. It is important to note here that the values of Θ_D, estimated from the resistivity measurement, found to be higher than that of the values extracted from the lattice thermal expansion and heat capacity data. We have already discussed that both longitudinal as well as transverse acoustic lattice vibrations were considered in the Debye model to calculate lattice specific heat theoretically. In contrast, only longitudinal phonons have been considered in the theory to develop Bloch-Grüneisen formula [45]. As the basic assumptions behind the Bloch-Grüneisen model and the Debye theory are quite different, consequently, the Debye temperature evaluated from electrical resistivity measurement differs from the Θ_D, obtained by the heat capacity data. However, the Θ_D (400 K), evaluated from lattice thermal expansion is found to be close enough to that of the heat capacity. It is important to note that the thermal expansion parameter (Θ_D) exhibit a Debye behaviour in the entire temperature region as the main contributions is provided by the phonons to thermal expansion. The coefficient of thermal expansion, α, is related to the heat capacity C and bulk modulus K_0 by $\alpha = (1/V)(\partial V/\partial T)_P = \gamma_G C/K_0 V$, where γ_G is Grüneisen parameter [34]. Generally, γ_G and K_0 have very weak

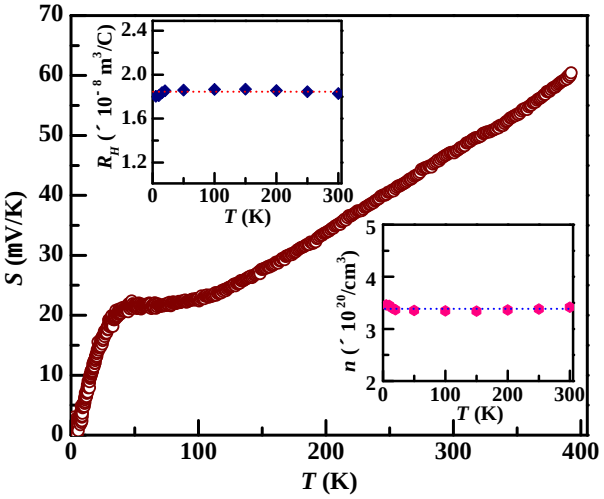

Figure 8: Temperature dependence of Seebeck coefficient of Ru_2TiGe. Insets: (a) Hall coefficient and (b) hole concentration as a function of temperature

dependence on temperature, the plot of α as a function of temperature essentially follows a Debye behavior. Because of these, the value of Θ_D estimated from the analysis of different data often found to differ in different analysis [45, 46]. Among all three Θ_D values of Ru_2TiGe, Θ_D = 407 K estimated from the heat capacity data is considered as the best representative of Θ_D in this system since the approximations considered in the Debye model, used to explain the temperature variation of heat capacity are most inclusive in nature.

3.4.2. Seebeck coefficient

In order to explore the thermoelectric properties of Ru_2TiGe, the temperature dependence of Seebeck coefficient [*S(T)*] has been investigated in the temperature range 2–390 K, as shown in Fig. 8. The value of Seebeck coefficient at 300 K is 47 μV/K, found to be higher than that of other Heusler alloys having VEC 24 like Fe_2VAl ($\sim$35 μV/K), Fe_2VGa ($\sim$30 μV/K), Ru_2NbAl ($\sim$22 μV/K) and Ru_2NbGa ($\sim$20 μV/K) [14, 53, 61, 62, 63, 64, 65]. The magnitude of the *S(T)* remains positive throughout the entire temperature region examined suggesting that the majority carriers for the thermoelectric transport must be holes in Ru_2TiGe. As the temperature raises, *S(T)* increases gradually and after exhibiting a hump-like shape with a maximum at $T \approx 50$ K, it varies almost linearly above 120 K and attains a value of 60 μV/K at 390 K. The *S(T)* onset of linear variations does not coincide with the onset of monotonous increase of the resistivity at around 80 K (Fig. 7). The maximum in *S(T)* rather matches with the lattice thermal conductivity maximum at 50 K (Fig. 9) discussed later. The appearance of the hump-like shape in *S(T)* curve of Ru_2TiGe can therefore be ascribed to the phonon drag effect, similar to that reported earlier in Fe_2TiSn [66]. However, the linear nature of *S(T)* curve at higher temperatures is in sync with observed metallic electric conduction behaviour of Ru_2TiGe.

3.4.3. Hall coefficient

The Hall coefficients (R_H) were measured for Ru_2TiGe in the temperature range 5–300 K for externally applied magnetic field of 50 kOe in order to check the sign of the Seebeck coefficient already discussed. The Hall resistivity increases with rising magnetic field almost with a constant slope for all the investigating temperatures and the value of R_H has been calculated using that constant slope. The magnitude of R_H remains positive and almost temperature independent for the entire temperature regime (Fig. 8, Inset:(a)) indicating the dominance of hole-type carrier for thermoelectric transport in conformity with the positive sign of *S(T)* observed in this compound (Fig. 8). The value of observed R_H is found to be $\sim 10^{-8}$ m^3/C, which is 100–1000 times larger than that of a conventional metals and nearly close to the elemental semimetals such as Sb. Similar values of R_H are also reported previously in the isoelectronic Heusler compounds Fe_2VAl ($\sim 2 \times 10^{-8}$) [61] and Fe_2VGa ($\sim 1 \times 10^{-8}$) [67]. Assuming the presence of only one type of carrier *i.e.* holes, the hole concentrations(n) are calculated $\sim 3.3 \times 10^{20}$ cm^{-3} (Fig. 8, Inset:(b)) using the relation $n = 1/eR_H$, where e is the charge of electron. Such carrier concentration is one order of magnitude smaller than that of the metallic Fe_2TiSn ($\sim 10^{21}$) [68] and subsequently 100–1000 times lower than a conventional metal. Having similar carrier concentration ($\sim 10^{20}$), isoelectronic Fe_2VAl and Fe_2VGa exhibit non-metallic electrical resistivity [61, 67]. In case of Ru_2TiGe, such small numbers of carriers are responsible for its low residual resistivity ratio and large thermopower that are indeed beneficial for achiving large zT.

3.4.4. Thermal conductivity

To further evaluate the thermoelectric performance of Ru_2TiGe, thermal conductivity

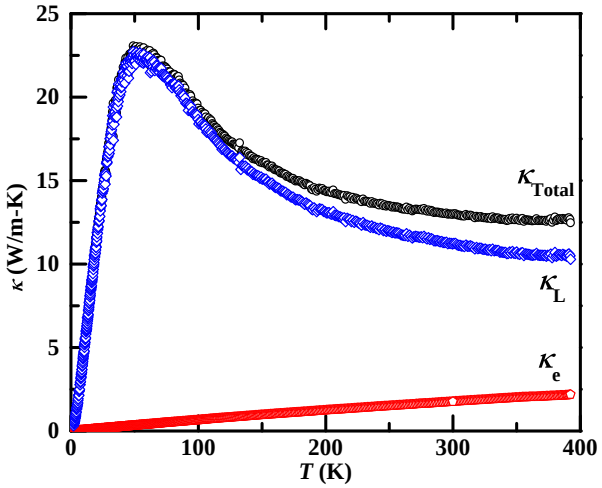

Figure 9: Temperature variations of the total thermal conductivity κ, lattice thermal conductivity κ_L, and electronic thermal conductivity κ_e for Ru_2TiGe as a function of temperature.

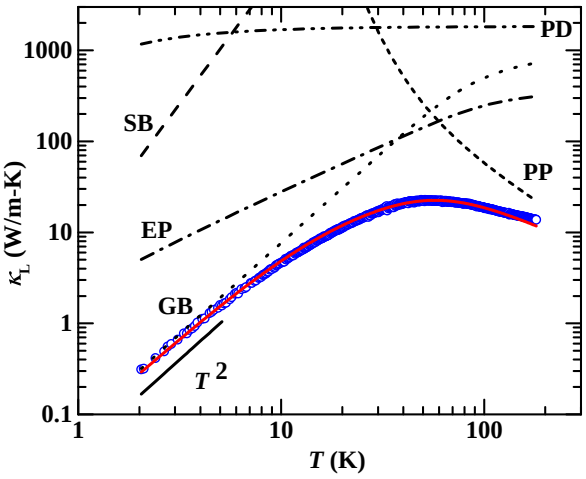

Figure 10: Temperature variations of lattice thermal conductivity κ_L for Ru_2TiGe. The open circles are the experimental data; the solid line is the fit to Eq. 10; the dashed curves are the theoretical limits on the lattice thermal conductivity imposed by different phonon scattering processes.

(κ) was measured in the temperature range 2–390 K (Fig. 9). At low temperatures, κ starts to increase rapidly with temperature and shows a sharp peak at ∼50 K. Above 50 K, the value of κ decreases and attains 12.4 W/m-K at 390 K (Fig. 9). For ordinary metals and semimetals, the total thermal conductivity is a sum of lattice (κ_L) and electronic (κ_e) contributions. The electronic thermal conductivity can be extracted using the Wiedemann-Franz law $\kappa_e\rho/T = L_0$, where ρ represents the measured dc electric resistivity and $L_0 = 2.45\times10^{-8}$ WΩK^{-2} is the Lorenz number. The lattice thermal conductivity κ_L can then be evaluated by subtracting κ_e from the observed κ. The estimated κ_e is found to be only a small contribution to κ (Fig. 9), indicating that the thermal conductivity of this material is essentially originated from κ_L (Fig. 9). At low temperatures, κ_L increases with temperature and a sharp maximum appears around 50 K because of the reduction in thermal scattering at low temperatures. The height of this peak in κ_L commonly represents the degree of crystallographic order in a compound and for a structurally disordered system this peak in κ_L remains absent [15, 69]. Thus, the sharp peak in κ_L for the present compound agrees with its ordered $L2_1$ structure. The κ_L value of Ru_2TiGe at 300 K is estimated to be 11.2 W/m-K (Fig. 9), which is however lower than those in Fe_2VAl (∼ 28 W/m-K) and Fe_2VGa (∼ 17 W/m-K) [62, 63, 64, 65]. This reduction may be attributed to smaller Debye temperature and speed of sound caused by substituting Fe by heavier Ru atom. Despite having a metal-like ground state, appreciably large value of thermopower as well as low κ in Ru_2TiGe increase the possibility of large zT in this compound.

In order to understand the influence of various phonon scattering mechanism on the lattice thermal conductivity of Ru_2TiGe, the $\kappa_L(T)$ data was analyzed using the Debye-Callaway model [70, 71]. According to this model, the lattice thermal conductivity as a function of temperature is described by the following equation:

$$\kappa_L(T) = \frac{k_B}{2\pi^2 v}\left(\frac{k_B T}{\hbar}\right)^3 \int_0^{\frac{\theta_D}{T}} \frac{x^4 e^x}{{\tau_P}^{-1}(e^x-1)^2}dx \quad (10)$$

where $x = \frac{\hbar\omega}{k_B T}$, ω and θ_D are the phonon frequency and the Debye temperature, respectively, and v represents the average phonon velocity that is approximately equal to the speed of sound in the studied material. The phonon scattering relaxation time, τ_P, is considered as the sum of different phonon scattering mechanism, defined as

$${\tau_P}^{-1} = \frac{v}{L} + A\omega^4 + B\omega^2 T e^{-\theta_D/3T} + C\omega + D\omega^2 \quad (11)$$

where L is the characteristic length defining the sample size and A, B, C and D are the free

Table 4: Parameters of the Debye-Callaway model fitted to the lattice thermal conductivity data in Ru_2TiGe. See main text for their definition.

A(s^3)	B(s/K)	C	D(s)
5.7×10^{-43}	5.5×10^{-18}	3.6×10^{-4}	3.3×10^{-17}

fitting parameters. The terms in the right of Eq. 11 are the scattering rates of phonon by the sample boundaries (SB), the point or mass defects (PD), the phonons (PP), the grain boundaries (GB) and the electrons (EP), respectively [70, 72, 73]. The frequency dependent expression ($C\omega$) for the phonon scattering rate by the grain boundaries has been included in Eq. 11 since κ_L shows a T^2 variation (Fig. 10) at very low temperature in Ru_2TiGe. Such T^2 variation of κ_L for silicon below ~70 K had previously been explained while deriving the above mentioned frequency dependent term $C\omega$ [72]. A metal-like ground state and the hole concentration of $\sim$ 3.3 $\times10^{20}$ cm^{-3}) in Ru_2TiGe compel to adapt the term $D\omega^2$ considering the phonon scattering rate by electron [73]. To fit the κ_L(T), the value of θ_D = 407 K estimated from the specific heat data is utilized and v = 3200 ms^{-1} is taken as the average speed of sound. Here, L = 2 mm was held as a fixed parameter giving its weak influence on the results.

A good agreement between the fitted curve and the measured values can be seen in Fig. 10. The deviation at the high temperature region most likely arises from radiation artifacts on the measurement. The fitted parameters are presented in Table 4. The relative weight of each scattering process on the lattice thermal conductivity can be better understood by replacing ${\tau_P}^{-1}$ in Eq. 10 by the individual scattering rate, yielding a theoretical limit imposed by each process on the lattice thermal conductivity. It can be interpreted from Fig. 10 that scattering by the sample boundaries and by the mass or point defects play a minor role in the κ_L of Ru_2TiGe. At low temperature, grain boundary scattering dominates while electron and phonon scattering play a major role at intermediate and high temperature regions, respectively.

3.4.5. Figure of merit

Using all three measured thermoelectric parameters *i.e.*, Seebeck coefficient [$S(T)$], electrical resistivity [$\rho(T)$] and thermal conductivity [$\kappa(T)$], the value of the power factor (PF=S^2/ρ) and the dimensionless figure of merit (zT=$S^2T/\rho\kappa$) are estimated and illustrated in Fig. 11. It should be mentioned here that the developement of superparamagnetic interaction below 20 K does not exhibit any noticeable influence in the power factor and figure of merit, as neither Seebeck coefficient nor thermal conductivity exhibit any discernible change in this temperature range. The small upturn in resistivity below 40 K is also likely to be due to the semiconducting nature. Additionally, since the practical application demands an improved zT value in the high temperature region ($T \geq$ 300 K), the effect of magnetism in the low temperature region may not have any practical significance. In the high temperature region, although Ru_2TiGe exhibits metal-like electric conduction, its comparably large Seebeck coefficient leads to achieve higher value of power factor (0.54 mW/mK^2 at 300 K) for this material than that of the existing Fe-based and other Ru-based stoichiometric Heusler alloys. For example, the room temperature PF values of 0.12 and 0.16 mW/mK^2 have been reported earlier in literature for Ru_2NbAl [14] and Fe_2VAl [69], respectively. With the rise of temperature, the PF curve after exhibiting a hump-like shape at around 40 K resulting from the phonon drag effect already observed in the $S(T)$ curve, increases and reaches at a value of 0.84 mW/mK^2 at 390 K. Such PF value for present compound is of the same order of magnitude to Fe_2VAl-based and Fe_2VGa-based Heusler alloys that are suitably doped for the

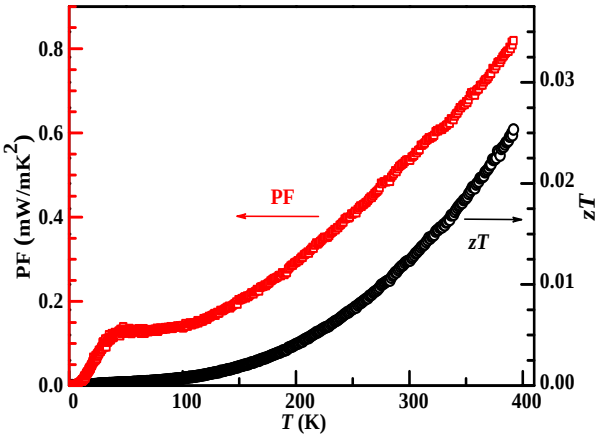

Figure 11: zT and power factor as a function of temperature for Ru_2TiGe.

improvisation of their zT values [56, 74, 75]. Similar to power factor, the estimated value of zT at 300 K (zT_{300K}= 0.012) is also higher than that of the most investigated non-doped thermoelectric material Fe_2VAl. The zT of Ru_2TiGe even exceeds the zT of Ru_2NbAl for which largest value of zT (0.0052 at 300 K) was obtained among all reported pristine Heusler compounds [14]. Temperature dependance of zT exhibit a increasing trend and yields almost two times higher value of 0.025 at 390 K than at 300 K. Nonetheless, it is still one order of magnitude smaller than that of the state-of-the-art thermoelectric material at 300 K, Bi_2Te_3 which displays zT = 0.8 at 300 K. Enhancement in zT values are earlier reported by suitable doping/substitution in proper site of the pristine Heusler alloys *viz.* Fe_2VAl, Ru_2NbGa, Ru_2TaAl *etc.* [16, 75, 76, 77]. It may be noted here that a 20-times increased zT value (0.036) at 300 K was reported in $Fe_2VAl_{0.9}Si_{0.1}$ [69] than in non-doped Fe_2VAl and by replacing heavier Ge atom in place of Si in $Fe_2VAl_{0.9}Si_{0.1}$, a total 72-fold increased zT value of 0.13 at 300 K was achieved in $Fe_2VAl_{0.9}Ge_{0.1}$ [63]. Interestingly, being only a pristine compound, Ru_2TiGe exhibits such a large value of zT at room temperature, further improvement in zT for Ru_2TiGe is highly anticipated by following similar strategy through doping to alter the metal-like ground state to a semiconductor-like one by adjusting the charge carrier concentration and substitution to reduce the lattice thermal conductivity.

4. Conclusion

An elaborate study on a Ru-based Heusler alloy, Ru_2TiGe, is performed through structural, magnetic, heat capacity and thermoelectric properties measurements. The magnetic properties at higher temperatures are dominated by temperature independent diamagnetic and Pauli paramagnetic contributions. In contrast to the observed magnetic behaviour at higher temperatures, superparamagnetic interaction among clusters is observed at lower temperatures below 20 K, despite the fact that none of the constituent atoms in Ru_2TiGe is usually known to order magnetically in nature. This short range magnetic interaction may have its origin in the small off-stoichiometry, noticed in otherwise structurally ordered (in $L2_1$ phase) Ru_2TiGe. Larger Hall coefficient ($R_H \sim 10^{-8}$ m^3/C), smaller Sommerfeld coefficient (γ_S = 0.2 mJ/mol-K^2) as well as lower RRR (ρ_{390K}/ρ_{2K}=1.22) than a conventional metal categorize Ru_2TiGe as a bad metal or a semi-metal. In spite of having a metal-like resistivity, a large value of Seebeck coefficient in this compound results in a larger power factor of the order of 0.54 mW/mK^2 at 300 K than that of the other reported non-doped Heusler alloys. Large power factor as well as low thermal conductivity which is the result of employing heavy constituent elements like Ru and Ge in Ru_2TiGe, give rise to a superior value of zT = 0.012 at 300 K in comparison to those reported in other pure Heusler alloys and point towards its high potential for practical thermoelectric applications. Adopting the strategies reported in literature for achieving many-fold increment of zT in Fe_2VAl through appropriate elemental substitution, similar great enhancement in the thermoelectric performances of Ru_2TiGe is also highly anticipated.

References

[1] H. Goldsmid, Thermoelectric refrigeration, Springer, 1964. doi:10.1007/978-1-4899-5723-8.

[2] Z. Dughaish, Lead telluride as a thermoelectric material for thermoelectric power generation, Physica B: Condensed Matter 322 (1-2) (2002) 205–223. doi:10.1016/s0921-4526(02)01187-0.

[3] G. Nolas, G. Slack, D. Morelli, T. Tritt, A. Ehrlich, The effect of rare-earth filling on the lattice thermal conductivity of skutterudites, Journal of Applied Physics 79 (8) (1996) 4002–4008. doi:10.1063/1.361828.

[4] H. Kleinke, New bulk materials for thermoelectric power generation: clathrates and complex antimonides, Chemistry of materials 22 (3) (2010) 604–611. doi:10.1021/cm901591d.

[5] Y. Huang, K. Hayashi, Y. Miyazaki, Enhancement of thermoelectric properties at room temperature through isoelectronic ruthenium-substitution in n-type half-heusler vfesb compounds, Acta Materialia 237 (2022) 118186. doi:10.1016/j.actamat.2022.118186.

[6] S. R. Culp, S. J. Poon, N. Hickman, T. M. Tritt, J. Blumm, Effect of substitutions on the thermoelectric figure of merit of half-Heusler phases at 800 C, Applied Physics Letters 88 (4) (2006) 042106. doi:10.1063/1.2168019.

[7] Y. Nishino, Thermoelectric properties of the pseudogap Fe_2VAl system, in: Materials Science Forum, Vol. 449, Trans Tech Publ, 2004, pp. 909–912. doi:10.4028/www.scientific.net/msf.449-452.909.

[8] T. Graf, C. Felser, S. S. Parkin, Simple rules for the understanding of heusler compounds, Progress in solid state chemistry 39 (1) (2011) 1–50 and references there in. doi:10.1016/j.progsolidstchem.2011.02.001.

[9] O. Heusler, Kristallstruktur und ferromagnetismus der mangan-aluminium-kupferlegierungen, Annalen der

Physik 411 (2) (1934) 155–201. doi:10.1002/andp.19344110205.

[10] Y. Nishino, M. Kato, S. Asano, K. Soda, M. Hayasaki, U. Mizutani, Semiconductorlike behavior of electrical resistivity in Heusler-type Fe_2VAl compound, Physical review letters 79 (10) (1997) 1909. doi:10.1103/physrevlett.79.1909.

[11] A. Ślebarski, J. Goraus, Electronic structure and thermodynamic properties of Fe_2VGa, Physical Review B 80 (23) (2009) 235121. doi:10.1103/physrevb.80.235121.

[12] A. Ślebarski, J. Deniszczyk, W. Borgieł, A. Jezierski, M. Swatek, A. Winiarska, M. Maple, W. Yuhasz, Electronic structure and thermodynamic properties of the Heusler alloys $Fe_2Ti_{1-x}V_xSn$, Physical Review B 69 (15) (2004) 155118. doi:10.1103/PhysRevB.69.155118.

[13] M. Mikami, Y. Kinemuchi, K. Ozaki, Y. Terazawa, T. Takeuchi, Thermoelectric properties of tungsten-substituted Heusler Fe_2VAl alloy, Journal of Applied Physics 111 (9) (2012) 093710. doi:10.1063/1.4710990.

[14] S. Mondal, C. Mazumdar, R. Ranganathan, E. Alleno, P. Sreeparvathy, V. Kanchana, G. Vaitheeswaran, Ferromagnetically correlated clusters in semimetallic Ru_2NbAl Heusler alloy and its thermoelectric properties, Physical Review B 98 (20) (2018) 205130. doi:10.1103/physrevb.98.205130.

[15] C. Kuo, H. Lee, C.-M. Wei, Y. Lin, Y. Kuo, C. Lue, Ru_2NbGa: A Heusler-type compound with semimetallic characteristics, Physical Review B 94 (20) (2016) 205116. doi:10.1103/physrevb.94.205116.

[16] C. Tseng, C. Kuo, H. Lee, K. Chen, R. Huang, C.-M. Wei, Y. Kuo, C. Lue, Semimetallic behavior in Heusler-type Ru_2TaAl and thermoelectric performance improved by off-stoichiometry, Physical Review B 96 (12) (2017) 125106. doi:10.1103/physrevb.96.125106.

[17] S. Mondal, C. Mazumdar, R. Ranganathan, Structural and transport properties of two new Heusler type Ru_2VAl and Ru_2VGa compounds, in: AIP Conference Proceedings, Vol. 1512, American Institute of Physics, 2013, pp. 978–979. doi:10.1063/1.4791369.

[18] S. Mondal, C. Mazumdar, R. Ranganathan, Ru_2VAl and Ru_2VGa: Two new heusler-type compounds, in: AIP Conference Proceedings, Vol. 1536, American Institute of Physics, 2013, pp. 825–826. doi:10.1063/1.4810482.

[19] B. Ramachandran, Y. Lin, Y. Kuo, C. Kuo, A. Gippius, C. Lue, Thermoelectric properties of Heusler-type $Ru_2VAl_{1-x}Ga_x$ alloys, Intermetallics 92 (2018) 36–41. doi:10.1016/j.intermet.2017.09.012.

[20] S. Krishnaveni, M. Sundareswari, Band gap engineering in ruthenium-based Heusler alloys for thermoelectric applications, International Journal of Energy Research 42 (2) (2018) 764–775. doi:10.1002/er.3864.

[21] I. Galanakis, P. Dederichs, N. Papanikolaou, Slater-Pauling behavior and origin of the half-metallicity of the full-Heusler alloys, Physical Review B 66 (17) (2002) 174429. doi:10.1103/physrevb.66.174429.

[22] C.-S. Lue, J. H. Ross Jr, K. Rathnayaka, D. Naugle, S. Wu, W. Li, Superparamagnetism and magnetic defects in Fe_2VAl and Fe_2VGa, Journal of Physics: Condensed Matter 13 (7) (2001) 1585. doi:10.1088/0953-8984/13/7/319.

[23] C. Lue, Y. Li, J. H. Ross Jr, G. M. Irwin, NMR and Mössbauer study of spin dynamics and electronic structure of $Fe_{2+x}V_{1-x}Al$ and Fe_2VGa, Physical Review B 67 (22) (2003) 224425. doi:10.1103/PhysRevB.67.224425.

[24] M. Vasundhara, V. Srinivas, V. Rao, Evidence for cluster glass behavior in Fe_2VAl Heusler alloys, Physical Review B 78 (6) (2008) 064401. doi:10.1103/physrevb.78.064401.

[25] Y. Feng, J. Rhee, T. Wiener, D. W. Lynch, B. Hubbard, A. Sievers, D. Schlagel, T. Lograsso, L. Miller, Physical properties of heusler-like Fe_2VAl, Physical Review B 63 (16) (2001) 165109. doi:10.1103/physrevb.63.165109.

[26] W. Gao, Z. Liu, T. Baba, Q. Guo, D.-M. Tang, N. Kawamoto, E. Bauer, N. Tsujii, T. Mori, Significant off-stoichiometry effect leading to the N-type conduction and ferromagnetic properties in titanium doped Fe_2VAl thin films, Acta Materialia 200 (2020) 848–856. doi:10.1016/j.actamat.2020.09.067.

[27] A. Ślebarski, M. Maple, E. Freeman, C. Sirvent, D. Tworuszka, M. Orzechowska, A. Wrona, A. Jezierski, S. Chiuzbaian, M. Neumann, Weak ferromagnetism induced by atomic disorder in Fe_2TiSn, Physical Review B 62 (5) (2000) 3296. doi:10.1103/physrevb.62.3296.

[28] S. Maier, S. Denis, S. Adam, J.-C. Crivello, J.-M. Joubert, E. Alleno, Order-disorder transitions in the Fe_2VAl Heusler alloy, Acta Materialia 121 (2016) 126–136. doi:10.1016/j.actamat.2016.08.080.

[29] J. Schaf, K. Le Dang, P. Veillet, I. Campbell, Extended and local effects of cold work in Heusler alloys, Journal of Physics F: Metal Physics 13 (6) (1983) 1311. doi:10.1088/0305-4608/13/6/028.

[30] J. Rodríguez-Carvajal, Recent advances in magnetic structure determination by neutron powder diffraction, Physica B: Condensed Matter 192 (1-2) (1993) 55–69. doi:10.1016/0921-4526(93)90108-i.

[31] M. Yin, P. Nash, Standard enthalpies of formation of selected Ru_2YZ Heusler compounds, Journal of Alloys and Compounds 634 (2015) 70–74. doi:10.1016/j.jallcom.2015.02.089.

[32] ASM Alloys database, https://matdata.asminternational.org/apd/index.aspx.

[33] Y. Sakai, M. Matoba, I. Yamada, K. Funakoshi, T. Kunimoto, Y. Higo, Y. Kamihara, New phases of binary compounds: CsCl-type RuGe and RuSn, EPL (Europhysics Letters) 107 (5) (2014) 56003. doi:10.1209/0295-5075/107/56003.

[34] F. Sayetat, P. Fertey, M. Kessler, An easy method for the determination of Debye temperature from thermal expansion analyses, Journal of applied crystallography 31 (2) (1998) 121–127. doi:10.1107/s0021889897006936.

[35] A. Iftikhar, A. Afaq, I. Ahmad, A. Bakar, H. B. Munir, N. ul Aarifeen, M. Asif, Computational Study of Ru_2TiZ (Z= Si, Ge, Sn) for Structural, Mechanical and Vibrational Properties, Zeitschrift für Naturforschung A 74 (6) (2019) 545–550. doi:10.1515/zna-2019-0054.

[36] P. E. Blanchard, E. Reynolds, B. J. Kennedy, J. A. Kimpton, M. Avdeev, A. A. Belik, Anomalous thermal expansion in orthorhombic perovskite $SrIrO_3$: Interplay between spin-orbit coupling and the crystal lattice, Physical Review B 89 (21) (2014) 214106. doi:10.1103/physrevb.89.214106.

[37] S. Mizusaki, A. Douzono, T. Ohnishi, T. Ozawa, Y. Noro, Y. Nagata, Metal–insulator–metal transition in Ti substituted antiferromagentic Ru_2MnGe Heusler alloy, Journal of alloys and compounds 553 (2013) 389–394. doi:10.1016/j.jallcom.2012.12.008.

[38] G. Cao, S. McCall, M. Shepard, J. Crow, R. Guertin, Thermal, magnetic, and transport properties of single-crystal $Sr_{1-x}Ca_x$ RuO_3 ($0 \leq x \leq 1.0$), Physical Review B 56 (1) (1997) 321. doi:10.1103/PhysRevB.56.321.

[39] A. Pandey, C. Mazumdar, R. Ranganathan, Magnetic behavior of binary intermetallic compound YPd_3, Journal of alloys and compounds 476 (1-2) (2009) 14–18. doi:10.1016/j.jallcom.2008.09.040.

[40] C. Hurd, Varieties of magnetic order in solids, Contemporary Physics 23 (5) (1982) 469–493. doi:10.1080/00107518208237096.

[41] D. I. Bilc, P. Ghosez, Electronic and thermoelectric properties of Fe_2VAl: the role of defects and disorder, Physical Review B 83 (20) (2011) 205204.

[42] C. Kittel, P. McEuen, P. McEuen, Introduction to solid state physics, Vol. 8, Wiley New York, 1996.

[43] A. Lonchakov, V. Marchenkov, S. Podgornykh, V. Okulov, K. Okulova, T. Govorkova, S. Emel'yanova, Examination of the specific features of the electron density of states of weakly nonstoichiometric Fe–V–Al alloys through the analysis of low-temperature heat capacity, Technical Physics Letters 42 (2016) 898–900. doi:10.1134/S1063785016090066.

[44] V. Okulov, A. Lonchakov, V. Marchenkov, Semiconductor-like behavior of electric transport in Fe–V–Al-based metallic alloys and their uncommon magnetic properties, Physics of Metals and Metallography 119 (2018) 1325–1328. doi:10.1134/S0031918X18130240.

[45] E. Gopal, Specific Heats at Low Temperatures, Springer, 1966. doi:10.1007/978-1-4684-9081-7.

[46] R. Goetsch, V. Anand, A. Pandey, D. Johnston, Structural, thermal, magnetic, and electronic transport properties of the $LaNi_2(Ge_{1-x}P_x)_2$ system, Physical Review B 85 (5) (2012) 054517. doi:10.1103/PhysRevB.85.054517.

[47] A. Hamri, Z. Dridi, B. Hamri, A. Hallouche, $Ru_2Ti_{1-x}Fe_xGe$: Novel candidate for the spintronic applications, International Journal of Modern Physics B 29 (09) (2015) 1550057. doi:10.1142/S0217979215500575.

[48] P. Anderson, E. Abrahams, T. Ramakrishnan, Possible explanation of nonlinear conductivity in thin-film metal wires, Physical Review Letters 43 (10) (1979) 718. doi:10.1103/physrevlett.43.718.

[49] B. Altshuler, A.G.Aronov, Electron-Electron Interaction In Disordered Conductors, in: A. Efros, M. Pollak (Eds.), Electron-Electron Interactions in Disordered Systems, Vol. 10 of Modern Problems in Condensed Matter Sciences, Elsevier, 1985, pp. 1–153. doi:10.1016/b978-0-444-86916-6.50007-7.

[50] G. Bergmann, Physical interpretation of weak localization: A time-of-flight experiment with conduction electrons, Physical Review B 28 (6) (1983) 2914. doi:10.1103/physrevb.28.2914.

[51] R. Kelekar, B. Clemens, Epitaxial growth of the Heusler alloy $Co_2Cr_{1-x}Fe_xAl$, Journal of applied physics 96 (1) (2004) 540–543. doi:10.1063/1.1759399.

[52] N. Mott, Conduction in glasses containing transition metal ions, Journal of Non-Crystalline Solids 1 (1) (1968) 1–17. doi:10.1016/0022-3093(68)90002-1.

[53] M. Vasundhara, V. Srinivas, V. Rao, Low-temperature electrical transport in Heusler-type $Fe_2V(AlSi)$ alloys, Journal of Physics: Condensed Matter 17 (38) (2005) 6025. doi:10.1088/0953-8984/17/38/008.

[54] J. Kondo, Resistance minimum in dilute magnetic alloys, Progress of theoretical physics 32 (1) (1964) 37–49. doi:10.1143/ptp.32.37.

[55] A. Lonchakov, V. Marchenkov, V. Okulov, K. Okulova, T. Govorkova, S. Podgornykh, New manifestations of a pseudogap state and electron spin scattering in the low-temperature thermal properties of near-stoichiometric iron-vanadium-aluminum alloys, Low temperature physics 41 (2) (2015) 150–153. doi:10.1063/1.4908195.

[56] M. Vasundhara, V. Srinivas, V. Rao, Electronic transport in Heusler-type $Fe_2VA_{1-x}M_x$ alloys (M = B, In, Si), Physical Review B 77 (22) (2008) 224415. doi:10.1103/PhysRevB.77.224415.

[57] J. Zhang, Y. Xu, S. Cao, G. Cao, Y. Zhang, C. Jing, Kondo-like transport and its correlation with the spin-glass phase in perovskite manganites, Physical Review B 72 (5) (2005) 054410. doi:10.1103/physrevb.72.054410.

[58] A. N. Pasupathy, R. C. Bialczak, J. Martinek, J. E. Grose, L. A. Donev, P. L. McEuen, D. C. Ralph, The Kondo effect in the presence of ferromagnetism, Science 306 (5693) (2004) 86–89. doi:10.1126/science.1102068.

[59] F. J. Blatt, Physics of electronic conduction in solids, McGraw-Hill, 1968.

[60] H. Huang, P. Qiu, Z. Gao, J. Xiao, X. Shi, L. Chen, Effect of cu-doping on the magnetic and electrical transport properties of three-quarter heusler alloy zrco1. 5sn, Journal of Applied Physics 129 (12) (2021) 125106.

[61] Y. Nishino, H. Kato, M. Kato, U. Mizutani, Effect of off-stoichiometry on the transport properties of the Heusler-type Fe_2VAl compound, Physical Review B 63 (23) (2001) 233303. doi:10.1103/physrevb.63.233303.

[62] C.-S. Lue, Y.-K. Kuo, Thermoelectric properties of the semimetallic Heusler compounds $Fe_{2-x}V_{1+x}M$ (M = Al, Ga), Physical Review B 66 (8) (2002) 085121. doi:10.1103/physrevb.66.085121.

[63] Y. Nishino, S. Deguchi, U. Mizutani, Thermal and transport properties of the Heusler-type $Fe_2VAl_{1-x}Ge_x$ ($0 \leq x \leq 0.20$) alloys: Effect of doping on lattice thermal conductivity, electrical resistivity, and Seebeck coefficient, Physical Review B 74 (11) (2006) 115115. doi:10.1103/physrevb.74.115115.

[64] C.-S. Lue, W. Lai, C. Chen, Y. Kuo, Off-stoichiometric effect on the transport and pseudogap characteristics of Fe_2VGa, Journal of Physics: Condensed Matter 16 (24) (2004) 4283. doi:10.1088/0953-8984/16/24/010.

[65] C.-S. Lue, J. Huang, D. Tsai, K. Sivakumar, Y. Kuo, Effects of Ge substitution on the thermoelectric properties and pseudogap characteristics of Fe_2VGa, Journal of Physics: Condensed Matter 20 (25) (2008) 255233. doi:10.1088/0953-8984/20/25/255233.

[66] C.-S. Lue, Y.-K. Kuo, Thermal and transport properties of the Heusler-type compounds $Fe_{2-x}Ti_{1+x}Sn$, Journal of applied physics 96 (5) (2004) 2681–2683. doi:10.1063/1.1776639.

[67] T. Fukuhara, H. Matsuda, S. Masubuchi, K. Ooiwa,

Y. Takano, F. Shimizu, K. Endo, Hall effect in heusler alloys fe2+ x v1-x al and fe2+ x v1-x ga, Journal of the Physical Society of Japan 73 (1) (2004) 13–16.

[68] I. Pallecchi, M. Pani, F. Ricci, S. Lemal, D. I. Bilc, P. Ghosez, C. Bernini, N. Ardoino, G. Lamura, D. Marré, Thermoelectric properties of chemically substituted full-heusler f e 2 tis n 1- x s b x (x= 0, 0.1, and 0.2) compounds, Physical Review Materials 2 (7) (2018) 075403.

[69] C. S. Lue, C. Chen, J. Lin, Y. Yu, Y. Kuo, Thermoelectric properties of quaternary Heusler alloys $Fe_2VAl_{1-x}Si_x$, Physical Review B 75 (6) (2007) 064204. doi:10.1103/physrevb.75.064204.

[70] J. Callaway, Model for lattice thermal conductivity at low temperatures, Physical Review 113 (4) (1959) 1046. doi:10.1103/physrev.113.1046.

[71] C. Walker, R. Pohl, Phonon scattering by point defects, Physical Review 131 (4) (1963) 1433. doi:10.1103/physrev.131.1433.

[72] Z. Wang, J. E. Alaniz, W. Jang, J. E. Garay, C. Dames, Thermal conductivity of nanocrystalline silicon: importance of grain size and frequency-dependent mean free paths, Nano letters 11 (6) (2011) 2206–2213. doi:10.1021/nl1045395.

[73] T. M. Tritt, Thermal conductivity: theory, properties, and applications, Springer Science & Business Media, 2005.

[74] P.-C. Wei, T.-S. Huang, S.-W. Lin, G.-Y. Guo, Y.-Y. Chen, Thermoelectric properties optimization of Fe_2VGa by tuning electronic density of states via titanium doping, Journal of Applied Physics 118 (16) (2015) 165102. doi:10.1063/1.4934734.

[75] K. Renard, A. Mori, Y. Yamada, S. Tanaka, H. Miyazaki, Y. Nishino, Thermoelectric properties of the Heusler-type $Fe_2VTa_xAl_{1-x}$ alloys, Journal of Applied Physics 115 (3) (2014) 033707. doi:10.1063/1.4861419.

[76] F. Garmroudi, M. Parzer, A. Riss, S. Beyer, S. Khmelevskyi, T. Mori, M. Reticcioli, E. Bauer, Large thermoelectric power factors by opening the band gap in semimetallic Heusler alloys, Materials Today Physics 27 (2022) 100742. doi:10.1016/j.mtphys.2022.100742.

[77] P. Bag, W. Liu, Y.-K. Kuo, C. Kuo, C. Lue, Thermoelectric properties of chemically substituted Heusler-type $Ru_{2-x}Nb_{1+x}Ga$ and $Ru_2NbGa_{1-x}M_x$ (M = In, Ge, and Sn) alloys, Journal of Alloys and Compounds 849 (2020) 156617. doi:10.1016/j.jallcom.2020.156617.